Nonlinear traveling waves in confined ferrofluids

Sérgio A. Lira and José A. Miranda*
Departamento de Física, Universidade Federal de Pernambuco, Recife, PE 50670-901 Brazil
(Received 2 August 2012; published 1 November 2012)

We study the development of nonlinear traveling waves on the interface separating two viscous fluids flowing in parallel in a vertical Hele-Shaw cell. One of the fluids is a ferrofluid and a uniform magnetic field is applied in the plane of the cell, making an angle with the initially undisturbed interface. We employ a mode-coupling theory that predicts the possibility of controlling the speed of the waves by purely magnetic means. The influence of the tilted magnetic field on the waves shape profile and the establishment of stationary traveling wave structures are investigated.

DOI: 10.1103/PhysRevE.86.056301 PACS number(s): 47.15.gp, 47.54.−r, 47.65.Cb, 47.20.Ma

I. INTRODUCTION

Frontal fluid flows in the confined geometry of a Hele-Shaw cell have been extensively investigated during the past five decades. Under frontal flow, the motion of the fluids is normal to the initially undisturbed interface between them and might lead to the formation of viscous fingering phenomena [1,2]. Curiously, the related problem of fluids flowing parallel to their separating interface and the development of interfacial traveling waves in the Hele-Shaw setup have been much less exploited in the literature [3–6]. Zeybek and Yortsos [3,4] studied parallel flow in a horizontal Hele-Shaw cell. In the limit of large capillary numbers and large wavelength they have found Korteweg–de Vries dynamics leading to stable finite-amplitude soliton solutions. Afterward, Gondret and co-workers [5,6] examined, through experiments and theory, the appearance of traveling waves for parallel flow in a vertical Hele-Shaw cell. They observed that the interface is destabilized above a certain critical flow velocity, so waves grow and propagate along the cell. Such waves are initially sinusoidal and then turn to localized structures presenting a nonlinear shape.

The theoretical model presented in Ref. [5] was based on a modified Darcy equation for the gap-averaged flow with an additional term representing inertial effects. Within this context a Kelvin-Helmholtz instability for inviscid fluids was found. For viscous fluids Gondret and Rabaud derived a Kelvin-Helmholtz-Darcy equation and verified that the threshold for instability was governed by inertial effects, while the wave velocity was determined by Darcy's law of flow of viscous fluids. Their theoretical analysis was backed up by their own experimental results. Theoretical improvements in the description of the system were proposed in Refs. [7–9], where the gap-averaged approach utilized in Ref. [5] was replaced by an alternative scheme directly based on the fully three-dimensional Navier-Stokes equation. In the end, the calculations in Refs. [7–9] lead to an equation of motion similar to the one derived in Ref. [5], but with slightly different coefficients.

One additional example of parallel flow in vertical Hele-Shaw cells is the linear stability analysis performed by Miranda and Widom [10]. The major differences between their work and the ones performed in Refs. [3–9] are that one of the fluids is a ferrofluid [11,12] and an external magnetic field is applied. The field could lie in the plane of the Hele-Shaw cell, either tangential or normal to the fluid-fluid interface. A ferrofluid is a stable colloidal suspension of nanometric magnetic particles that behaves as a regular viscous fluid except that it can experience forces due to magnetic polarization [13]. This opens up the possibility of investigating the role played by the magnetic field in the dynamics of the parallel flow. It has been shown [10] that the dispersion relation governing mode growth is modified so that the magnetic field can destabilize the interface even in the absence of inertial effects. However, it has been deduced that the magnetic field would not affect the speed of wave propagation. Despite all that, a study addressing the effect of the magnetic field on the morphological structure and nonlinear evolution of the propagating waves is still lacking.

In this work we reexamine the problem initially proposed in Ref. [10] by considering the action of an in-plane tilted applied magnetic field that makes an arbitrary angle with the direction defined by the unperturbed fluid-fluid interface. This apparently naive modification proves to be crucial in creating a connection between the applied field and the propagating wave velocity. Moreover, in contrast to what was done in Ref. [10], we go beyond the linear regime and tackle the problem by using a perturbative weakly nonlinear approach. This particular theoretical tool enables one to extract valuable analytical information at the onset of nonlinearity. As a consequence, one can investigate the influence of the magnetic field on the nonlinear dynamics and the ultimate shape of the traveling surface waves.

The layout of this work is as follows. Section II introduces the governing equations of the parallel flow system with a ferrofluid and presents our mode-coupling approach, which is valid at the lowest nonlinear perturbative order [14,15]. Linear and weakly nonlinear dynamics are discussed in Sec. III. We show that the effect of the magnetic field on the velocity and shape of the propagating waves can be accessed by considering the interplay of a small number of Fourier modes. One important result is the feasibility of sustaining, moving, and controlling a traveling wave solely under the action of an external magnetic field. Stationary wave profiles are found for different values of the magnetic field tilting angle. Our main conclusions are summarized in Sec. IV.

*jme@df.ufpe.br

II. PROBLEM FORMULATION AND GOVERNING EQUATIONS

Consider two semi-infinite immiscible viscous fluids, flowing with velocities U_j, where $j = 1$ ($j = 2$) labels the lower (upper) fluid. The flow takes place along the x direction in a vertical Hele-Shaw cell of thickness b (Fig. 1). The densities and viscosities of the fluids are denoted by ρ_j and η_j, respectively. The cell lies parallel to the xy plane, where the y axis is vertical. Between the fluids there exists a surface tension σ; the lower fluid is assumed to be a ferrofluid (magnetization $\mathbf{M}$), whereas the upper fluid is nonmagnetic (zero magnetization). The acceleration of gravity $\mathbf{g} = -g\hat{\mathbf{y}}$, where $\hat{\mathbf{y}}$ is the unit vector on the y axis. The base flow is horizontal with $\eta_1 U_1 = \eta_2 U_2$ [5] because the flows in the two fluids are driven by the same pressure gradient.

A uniform external magnetic field $\mathbf{H}_0 = H_0(\cos\alpha\hat{\mathbf{x}} + \sin\alpha\hat{\mathbf{y}})$ is applied in the plane of the cell. The shape of the perturbed fluid-fluid interface is described as $\mathcal{I}(x,y,t) = y - \zeta(x,t) = 0$, where $\zeta(x,t) = \sum_{k=-\infty}^{+\infty} \zeta_k(t)\exp(ikx)$ represents the net interface perturbation with Fourier amplitudes $\zeta_k(t)$ and wave numbers k.

For the quasi-two-dimensional geometry of the Hele-Shaw cell, the three-dimensional fluid flow is reduced to an equivalent two-dimensional one by averaging the Navier-Stokes equation over the direction perpendicular to the plates. Using no-slip boundary conditions and neglecting inertial terms, the flow in such a confined environment is governed by a modified Darcy law [16–19]

$$\mathbf{v}_j = -\frac{b^2}{12\eta_j}\left\{\nabla p_j - \frac{1}{b}\int_{-b/2}^{b/2}\mu_0(\mathbf{M}\cdot\nabla)\mathbf{H}\,dz + \rho_j g\hat{\mathbf{y}}\right\}, \tag{1}$$

where p_j denotes the pressure. The local magnetic field appearing in Eq. (1) differs from the applied field $\mathbf{H}_0$ by a demagnetizing field of the polarized ferrofluid $\mathbf{H} = \mathbf{H}_0 + \mathbf{H}_d$, where $\mathbf{H}_d = -\nabla\varphi$, with φ a scalar magnetic potential. Since $\mathbf{H}_0$ is spatially uniform it eventually drops out in the calculation of the magnetic term in Eq. (1) and the magnetic effects are actually due to the demagnetizing field.

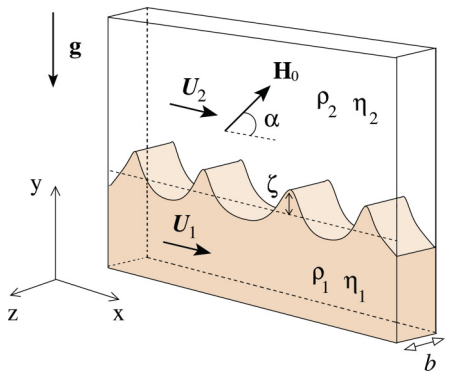

FIG. 1. (Color online) Schematic configuration of the parallel flow in a vertical Hele-Shaw cell. The lower fluid is a ferrofluid, while the upper fluid is nonmagnetic. An external uniform magnetic field $\mathbf{H}_0$ is applied, making an angle α with the initially undisturbed interface separating the fluids.

The role of inertia in the problem can be quantified by a Reynolds number (relative measure of inertial and viscous forces) that is directly proportional to the cell gap thickness and inversely proportional to the viscosity of fluid $\mathrm{Re}_j = \rho_j U_j b/12\eta_j$. Since most experimental and theoretical studies of ferrofluid flow in Hele-Shaw cells deal with very thin cell gaps and highly viscous fluids, the vanishing Reynolds number limit is readily validated. Under such circumstances, the fluid motion is perfectly described by the gap-averaged modified Darcy law (1). As discussed in Refs. [5,20,21] in unidirectional Hele-Shaw parallel flow, the inertial effects can be neglected, even at relatively large Reynolds numbers as long as $\mathrm{Re}_j < \mathrm{Re}_c$, where Re_c is the Reynolds number corresponding to the laminar-turbulent transition.

We follow the standard approximations used by other researchers [11,12,16,17,22,23] and assume that the ferrofluid is magnetized such that its magnetization is collinear with the applied field $\mathbf{M}(\mathbf{H}) = M(\cos\alpha\hat{\mathbf{x}} + \sin\alpha\hat{\mathbf{y}})$, where $M = M(H_0)$. Only the lowest-order effect of the magnetic interactions that would result in fluid motion is considered. As originally proposed by Tsebers and Maiorov [22], we assume that the magnetization of the magnetic fluid in a uniform magnetic field is both uniform and constant. We emphasize that although the magnetization is taken to be uniform, the demagnetizing field is not, as discussed in Refs. [17,23–25].

Taking into consideration the physical assumptions mentioned above and the particular geometry of our system, Eq. (1) can be rewritten as

$$\mathbf{v}_j = -\frac{b^2}{12\eta_j}\nabla\left\{p_j + \rho_j g y + \mu_0\frac{M}{b}\int_{-b/2}^{b/2}\left[\cos\alpha\frac{\partial\varphi}{\partial x} + \sin\alpha\frac{\partial\varphi}{\partial y}\right]dz\right\}, \tag{2}$$

where

$$\varphi = \frac{1}{4\pi}\int_{\mathcal{S}}\frac{\mathbf{M}\cdot\mathbf{n}'}{|\mathbf{r}-\mathbf{r}'|}d^2r' = \frac{1}{4\pi}\int_{-\infty}^{+\infty}\int_{-b/2}^{b/2}\frac{M(\cos\alpha\hat{\mathbf{x}} + \sin\alpha\hat{\mathbf{y}})\cdot\mathbf{n}'dx'dz'}{\sqrt{(x-x')^2 + (y-y')^2 + (z-z')^2}}. \tag{3}$$

The unprimed coordinates $\mathbf{r}$ denote arbitrary points in space, the primed coordinates $\mathbf{r}'$ are integration variables within the magnetic domain $\mathcal{S}$, and $d^2r' = dx'dz'$ denotes the infinitesimal area element. The vector $\mathbf{n}'$ represents the unit normal to the magnetic domain under study.

By inspecting Eq. (2) we observe that the velocity depends on a linear combination involving gradients of hydrodynamic pressure, gravity, and magnetic potential, respectively. Thus the term in curly brackets in Eq. (2) can be seen as an effective pressure. Therefore, as in the Hele-Shaw problem with nonmagnetic fluids [1,2], the flow is potential $\mathbf{v}_j = -\nabla\phi_j$, but now with a velocity potential given by

$$\phi_j = \frac{b^2}{12\eta_j}\{p_j - \mu_0 M^2 I(x,y) + \rho_j g y\}, \tag{4}$$

where

$$I(x,y)=\frac{1}{4\pi b}\int_{-\infty}^{\infty}\int_{-b/2}^{b/2}\int_{-b/2}^{b/2}\frac{-\cos\alpha\frac{\partial\zeta(x')}{\partial x'}+\sin\alpha}{\sqrt{1+\left(\frac{\partial\zeta(x')}{\partial x'}\right)^2}}\times\frac{\{\cos\alpha(x-x')+\sin\alpha[y-\zeta(x')]\}dx'dz'dz}{\sqrt{(x-x')^2+[y-\zeta(x')]^2+(z-z')^2}}. \tag{5}$$

In Eq. (5) the integral in dz is related to the gap-average calculation [see Eq. (2)], while the integrals in dx' and dz' come from the surface integral in the magnetic domain of interest $\mathcal{S}$ [see Eq. (3)]. Notice that incompressibility ($\nabla\cdot\mathbf{v}_j=0$) then yields Laplace's equation for the velocity potential.

The problem is specified by two boundary conditions

$$p_1-p_2=\sigma\kappa-\tfrac{1}{2}\mu_0(\mathbf{M}\cdot\mathbf{n})^2, \tag{6}$$

$$\mathbf{n}\cdot\nabla\phi_1=\mathbf{n}\cdot\nabla\phi_2. \tag{7}$$

Equation (6) is an augmented pressure jump condition at the interface, where κ denotes the interfacial curvature. A crucial difference of this expression from the one utilized in the nonmagnetic situation is given by the second term on the right-hand side: the so-called magnetic normal traction [11,12], which considers the influence of the normal component of the magnetization at the interface. For the current field configuration this magnetic piece is at least of second order in ζ, being legitimately nonlinear. This magnetic term contributes to determine the shape of the traveling wave profiles at the onset of nonlinear effects. The second boundary condition (7) simply states the continuity of the normal flow velocity at the interface.

Our next task is to derive an equation of motion for the perturbation amplitudes that is able to capture the essential physics at the lowest nonlinear level. This is done by following standard steps performed in previous weakly nonlinear studies [14,15,18]. First, we define Fourier expansions for the velocity potentials. Then we express ϕ_j in terms of the perturbation amplitudes ζ_k by considering the kinematic boundary condition (7). Substituting these relations and the modified pressure jump condition (6) into Eq. (4), always keeping terms up to second order in ζ, and Fourier transforming, we find the dimensionless equation of motion (for $k\neq 0$)

$$\dot{\zeta}_k=\Lambda(k)\zeta_k+\sum_{k'\neq 0}[F(k,k')\zeta_{k'}\zeta_{k-k'}+G(k,k')\dot{\zeta}_{k'}\zeta_{k-k'}], \tag{8}$$

where the overdot denotes total time derivative,

$$\Lambda(k)=\lambda(k)-ik\left[c_0+N_B|k|\frac{\sin 2\alpha}{2}\right] \tag{9}$$

is a complex linear growth rate, and

$$\lambda(k)=|k|\{N_B[\sin^2\alpha\,W_1(k)-\cos^2\alpha\,W_2(k)]-k^2-N_G\} \tag{10}$$

is its real part.

The system is characterized by three dimensionless parameters

$$N_B=\frac{\mu_0M^2b}{\sigma},\quad N_G=\frac{(\rho_1-\rho_2)gb^2}{\sigma},\quad c_0=\frac{12(\eta_1U_1+\eta_2U_2)}{\sigma}.$$

The magnetic Bond number N_B measures the ratio of magnetic to capillary forces, while the gravitational Bond number N_G accounts for the relative importance of the gravitational force to the surface tension. The parameter c_0 represents the propagation contribution due to the parallel flow. Notice that c_0 can be seen as a modified capillary number $\mathrm{Ca}=\mathrm{Ca}_1+\mathrm{Ca}_2$, where $\mathrm{Ca}_j=12\eta_jU_j/\sigma$ is the capillary number of fluid j. In addition,

$$W_1(k)=\frac{1}{\pi}\int_0^{\infty}\frac{(1-\cos k\tau)}{\tau^2}[\sqrt{\tau^2+1}-\tau]d\tau \tag{11}$$

and

$$W_2(k)=\frac{k}{\pi}\int_0^{\infty}\frac{\sin k\tau}{\tau}[\sqrt{\tau^2+1}-\tau]d\tau \tag{12}$$

originate from the contribution of the demagnetizing field.

The second-order mode-coupling terms are given by

$$F(k,k')=N_B|k|\frac{k'(k'-k)}{2}\left\{\cos 2\alpha+i\sin 2\alpha\left[\frac{W_1(k')}{k'}-\frac{W_2(k)}{2k}+\frac{W_3(k,k')}{k'(k'-k)}\right]\right\} \tag{13}$$

and

$$G(k,k')=A|k|[\mathrm{sgn}(kk')-1], \tag{14}$$

where

$$W_3(k,k')=\frac{1}{\pi}\int_0^{\infty}[\sin k\tau-\sin k'\tau-\sin(k-k')\tau]\times\left\{\frac{[\sqrt{\tau^2+1}-\tau]}{\tau^4}+\frac{1}{2\tau}\left[\frac{1}{\tau}-\frac{1}{\sqrt{\tau^2+1}}\right]\right\}d\tau \tag{15}$$

is another demagnetizing integral. Notice the presence of the imaginary part in Eq. (13) that is proportional to N_B and $\sin 2\alpha$ and would vanish for a purely vertical or horizontal magnetic field. The sign function equals ± 1 according to the sign of its argument and the viscosity contrast is defined as $A=(\eta_1-\eta_2)/(\eta_1+\eta_2)$. In Eqs. (8)–(15) the lengths and velocities are rescaled by b and $\sigma/[12(\eta_1+\eta_2)]$, respectively. Without loss of generality we focus on the situation in which $\rho_1>\rho_2$ and $\eta_1\gg\eta_2$, so the interface is gravitationally stable ($N_G>0$) and $A\approx 1$. Since the gravitational Bond number plays a minor role in our analysis, for the rest of this work we set its value as $N_G=1.4$. We recover the results for the vertical magnetic field configuration without flow, previously studied in Ref. [18], by setting $\alpha=\pi/2$ and $c_0=0$. It should be noted that the theoretical results presented in the following section utilize dimensionless quantities that are extracted from the realistic physical parameters used in the experiments of Refs. [5,19].

III. PROPAGATING WAVES: DYNAMICS, MORPHOLOGY, AND STABILITY

A. Linear regime

Before examining how we can use the mode-coupling equation (8) to access important nonlinear aspects related to the traveling waves, we briefly discuss a few useful concepts associated with the linear growth rate (9). The real part of the growth rate $\mathrm{Re}[\Lambda(k)] = \lambda(k)$ governs the exponential growth or decay of the wave amplitudes at the linear regime. Since a positive $\lambda(k)$ leads to an unstable behavior, Eq. (10) tells us that the term $W_1(k)$ $[W_2(k)]$, which is proportional to N_B and represents the contribution of the vertical (horizontal) magnetic field component, is destabilizing (stabilizing). In contrast, gravity and surface tension try to stabilize interfacial disturbances. The interplay of these competing effects determines the linear stability of the initially flat fluid-fluid interface. This is illustrated in Fig. 2, which plots $\lambda(k)$ in terms of k for two values of N_B and three increasingly larger values of the angle α. By inspecting Eq. (10) it is clear that the magnetic field (demagnetizing field contribution) causes the instability, even in the absence of inertial effects [10,18].

It is evident from Fig. 2 that, for a given magnetic Bond number and by increasing α, the transition from a stable to an unstable situation occurs when $\lambda(k) = 0$ and $d\lambda(k)/dk = 0$, which defines a critical value for α. Moreover, the maximum of $\lambda(k)$ takes place at $k = k_{\max}$, which characterizes the dominant wave number of the emergent pattern. It increases and moves towards higher values of k as α approaches $\pi/2$. The behavior of $\lambda(k)$ as a function of α is magnified by increasing N_B. We point out that in order to observe any instability band, N_B must be above the critical value given by the vertical field situation ($N_B > 11.12$) [18].

The behavior of $k_{\max}$ as a function of α is depicted in Fig. 3. Here we see that as α approaches $\pi/2$ ($\alpha \approx 1.57$), $k_{\max}$ reaches a maximum possible value for a given N_B. The critical values of α are marked with dots and vertical dashed lines. By increasing the magnetic field the curves move upward and the critical values of α decrease.

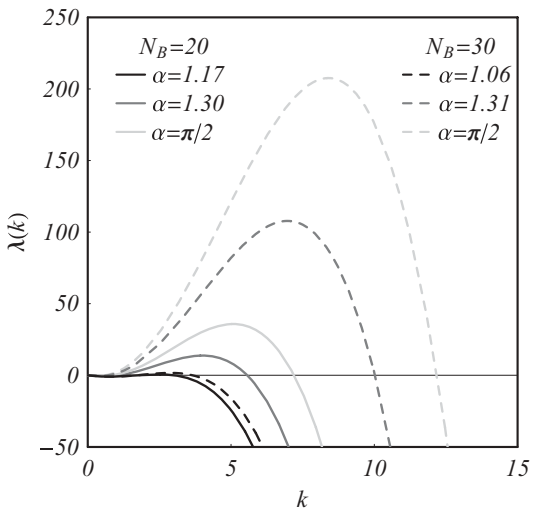

FIG. 2. Real part of the linear growth rate $\lambda(k)$ as a function of the wave number k for $N_G = 1.4$. Continuous (dashed) curves refer to $N_B = 20$ ($N_B = 30$). For each N_B we plot curves for three values of the angle α, where lighter gray curves correspond to higher values of α.

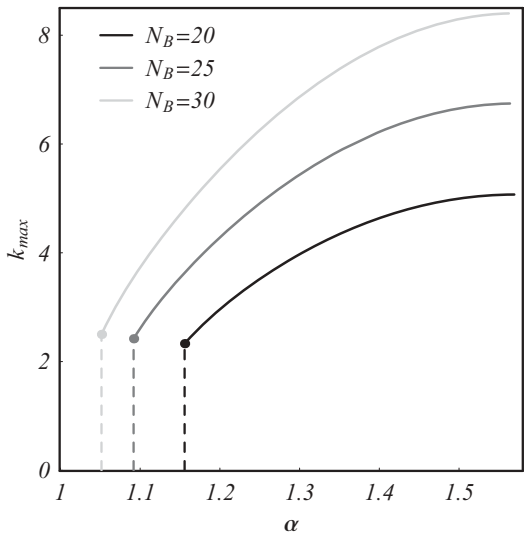

FIG. 3. Dominant wave number $k_{\max}$ as a function of the angle α for $N_G = 1.4$ and three different values of N_B. The dots indicate the critical values of α below which the interface is stable.

The imaginary part of the growth rate (9) $\mathrm{Im}[\Lambda(k)]$ divided by $-k$ gives us the phase velocity of perturbations at the linear regime. It presents a parallel flow contribution represented by c_0 and a magnetic one proportional to N_B that comes from the fact that the magnetic field has nonzero x and y components. This last term is very important for our analysis of propagating profiles and would not be present if the magnetic field was simply vertical ($\alpha = \pi/2$) or horizontal ($\alpha = 0$) as considered in Ref. [10]. In order to detect any influence of the magnetic field on the phase velocity we must consider the interval between these two limiting situations ($0 < \alpha < \pi/2$). From these comments the key role played by the tilted magnetic field becomes evident: Now one could have wave propagation even if $c_0 = 0$ and it would be exclusively due to magnetic effects.

B. Weakly nonlinear dynamics

At this point we turn our attention to the weakly nonlinear, intermediate stages of interfacial pattern evolution. We use the equation of motion (8) to investigate how the magnetic field influences the shape and velocity of the propagating waves. We employ a theoretical approach originally proposed in Refs. [14,15] and focus on a mechanism controlling the interface behavior through magnetic means. This is done by considering the coupling of a small number of modes. For a given α larger than the critical value, only discrete modes, in multiples of the dominant wave number $k_{\max}$, are selected due to translational invariance. In this framework we examine the interaction of the fundamental mode k with its own harmonic $2k$. For the rest of this work we consider values of α above the critical situation and take the fundamental wave number $k = k_{\max}$ as the fastest growing mode.

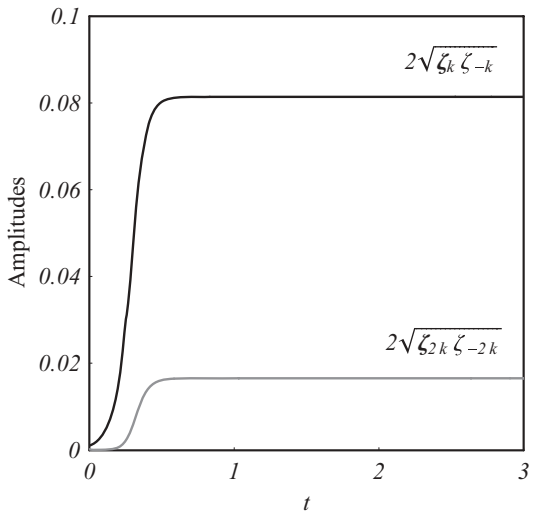

FIG. 4. Numerical time evolution of the absolute value of the perturbation amplitudes for the fundamental mode $2\sqrt{\zeta_k\zeta_{-k}}$ and its first harmonic $2\sqrt{\zeta_{2k}\zeta_{-2k}}$. The parameters considered correspond to the continuous dark gray curve in Fig. 2 ($N_G = 1.4$, $c_0 = 0.5$, $N_B = 20$, and $\alpha = 1.30$). As time increases, the amplitudes tend to saturate and reach stationary values, indicating the propagation of an unchanged shape profile.

Considering these two modes, the moving interface profile can be described as

$$\zeta(x,t) = \zeta_k(t)\exp(ikx) + \zeta_{-k}(t)\exp(-ikx) + \zeta_{2k}(t)\exp(2ikx) + \zeta_{-2k}(t)\exp(-2ikx), \quad (16)$$

with ζ_k and ζ_{-k} (also ζ_{2k} and ζ_{-2k}) being complex conjugates. Specifically, one needs to solve the coupled nonlinear differential equations

$$\dot{\zeta}_{2k} = \Lambda(2k)\zeta_{2k} + [F(2k,k)\zeta_k + G(2k,k)\dot{\zeta}_k]\zeta_k, \quad (17)$$

$$\dot{\zeta}_k = \Lambda(k)\zeta_k + [F(k,-k)\zeta_{-k} + G(k,-k)\dot{\zeta}_{-k}]\zeta_{2k} + [F(k,2k)\zeta_{2k} + G(k,2k)\dot{\zeta}_{2k}]\zeta_{-k}. \quad (18)$$

The interface evolution is obtained by numerically solving Eqs. (17) and (18). We have verified that the amplitudes and relative phase of the solutions saturate for later times, leading to stationary propagating profiles. Figure 4 shows the time evolution of the absolute value of the perturbation amplitudes. We consider very low initial amplitude values ($\zeta_k = 0.001$ and $\zeta_{2k} = 0.0001$) and parameters $N_G = 1.4$, $c_0 = 0.5$, $N_B = 20$, and $\alpha = 1.30$. This figure depicts the amplitude's evolution beginning from a nearly flat interface, exponentially growing at the linear stage, and then saturating at later times. Thus, after a transient period of growth the perturbation amplitudes remain unchanged as time progresses. The main difference between these findings and the results in Ref. [18] is that here the saturated modes ζ_k and ζ_{2k} now maintain a locked phase difference between them in such a way to lead to a steady profile propagation. It is also evident from Fig. 4 that the weakly nonlinear coupling naturally dictates the enhanced growth of a positive harmonic mode.

An example of a steady propagating profile found numerically is plotted in Fig. 5 for $N_G = 1.4$, $c_0 = 0.5$, $N_B = 20$, and

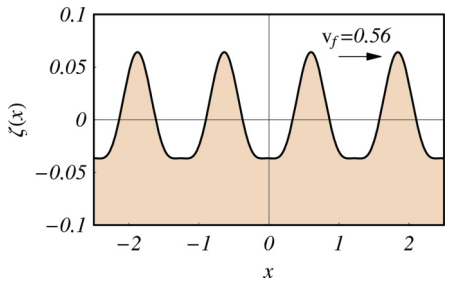

FIG. 5. (Color online) Propagating wave profile for $c_0 = 0.5$, $N_B = 20$, and $\alpha = \pi/2$, resulting in $v_f = 0.56$. The profile and velocity are reflected in relation to the y axis if we perform the transformation $c_0' = -c_0$.

$\alpha = \pi/2$ ($k_{\max} = 5.07$). Its real growth rate is represented by the light gray solid curve in Fig. 2. The resulting wave pattern shows a sequence of sharp peaked structures separated by wider troughs. These shapes are similar to the ones obtained in the situation in which there is no parallel flow and the magnetic field is vertical [18]. There is little morphological difference produced by the introduction of the parallel flow, represented by a nonvanishing c_0, if $\alpha = \pi/2$, but now we have a propagating profile instead of a stationary one. We define v_f as the final propagation velocity of the saturated profile, which in Fig. 5 equals 0.56. Note that v_f is not given solely by the linear phase velocity in Eq. (9), but it is a result of the weakly nonlinear coupling between the modes in the saturated regime.

Since c_0 has very little influence on the morphology of the rising wave patterns (independently of the angle α), we take $c_0 = 0$ in Fig. 6 and focus on the role of the magnetic field tilting angle α in determining the morphology of the propagating solutions. In practical terms, for finite surface tension flows, the limit $c_0 = 0$ can be obtained by setting the velocities $U_1 = U_2 = 0$. For α close to the critical value, as shown in Fig. 6(a), the solution is dominated by the fundamental mode and the shape of the profile resembles a pure propagating cosine wave. As α increases, the wave morphology changes and we see a series of slightly inclined peaks, as exemplified in Fig. 6(b). This is possible due to the significant magnitude of the first harmonic mode. For higher values of α we get peaked structures similar to the ones depicted in Fig. 5 (where $\alpha = \pi/2$). Notice that it is sufficient to explore the influence of the tilted magnetic field in the range $0 \leqslant \alpha \leqslant \pi/2$. This is justified by the fact that the propagating wave problem is reflected in relation to the y axis under the transformation $\alpha' = \pi - \alpha$ and is symmetric under the transformation $\alpha' = \pi + \alpha$. Complementary information about the influence of α on the magnitude of the final propagating velocities will be exploited in the discussion of Fig. 7.

C. Analytical approach to steady solutions

In order to have a more quantitative account of the propagating steady profiles numerically predicted in Sec. III B, we now carry out an analytical study, aiming to find wave solutions to our problem, and analyze their stability.

To obtain a steady propagating solution we impose that $\zeta(x,t) = \zeta(kx - \omega t)$, where ω is real and $v_f = \omega/k$

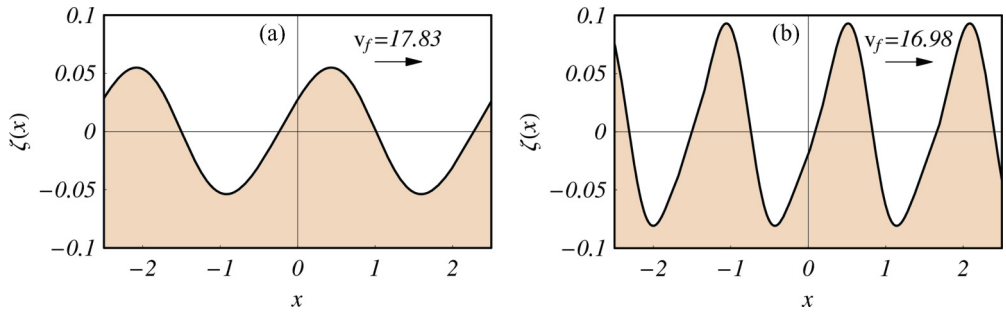

FIG. 6. (Color online) (a) Propagating wave profile for $N_B = 20$ and $\alpha = 1.17$, resulting in $v_f = 17.83$. (b) Propagating wave profile for $N_B = 20$ and $\alpha = 1.30$, resulting in $v_f = 16.98$. The profile and velocity are reflected in relation to the y axis if we perform the transformation $\alpha' = \pi - \alpha$. Note that here $c_0 = 0$.

is the final propagating velocity. Therefore, we can write $\zeta_k(t) = c_1 \exp(-i\omega t)$ and $\zeta_{2k}(t) = c_2 \exp(-i2\omega t)$ as propagating modes with constant amplitudes. We may take c_1 as a real constant without loss of generality since an imaginary part of it would simply translate the resulting profile. However, we keep c_2 as a complex number, so there is a phase difference between the modes ζ_k and ζ_{2k}, something that is relevant for the profile morphology. By inserting these conditions into Eqs. (17) and (18) we get a complete set of nonlinear time-independent equations that determine c_1, c_2, and ω [see Eqs. (A1) and (A2) in the Appendix].

By manipulating the equations of the system described above we find a cubic algebraic equation for ω with real coefficients that depends on the functions expressed by Eqs. (9)–(15). We have verified that within our range of physical parameters (taken from the experiments in Refs. [5,19]), this polynomial equation has a positive discriminant and therefore three different real roots are found (see the Appendix for details). To find out which of these solutions gives the actual propagating velocity we perform a stability analysis of the propagating solution by perturbing the modes' stationary amplitudes $\zeta_k(t) = (\epsilon_1 + c_1)\exp(-i\omega t)$ and $\zeta_{2k}(t) = (\epsilon_2 + c_2)\exp(-i2\omega t)$, with $\epsilon_1 = \epsilon_1(t)$ real and $\epsilon_2 = \epsilon_2(t)$ complex. By inserting these conditions in Eqs. (17) and (18) and expanding up to first order in ϵ, the stability analysis of the solution leads to a set of equations that can be expressed in a matrix form as

$$\begin{pmatrix} \dot{\epsilon}_1 \\ \dot{\epsilon}_2 \end{pmatrix} = \begin{pmatrix} \mathcal{A}_{11} & \mathcal{A}_{12} \\ \mathcal{A}_{21} & \mathcal{A}_{22} \end{pmatrix} \begin{pmatrix} \epsilon_1 \\ \epsilon_2 \end{pmatrix}, \tag{19}$$

where

$$\mathcal{A}_{11} = \frac{\Lambda(k) + i\omega + [F(k,-k) + F(k,2k) + iG(k,-k)\omega]c_2}{1 - G(k,-k)c_2},$$

$$\mathcal{A}_{12} = \frac{[F(k,-k) + F(k,2k)]c_1 + iG(k,-k)\omega c_1}{1 - G(k,-k)c_2},$$

$$\mathcal{A}_{21} = 2F(2k,k)c_1,$$

$$\mathcal{A}_{22} = \Lambda(2k) + i2\omega.$$

If the real part of an eigenvalue of the matrix $\mathcal{A}$ is positive (negative), it indicates that there is an unstable (stable) branch of the dynamic system defined by Eqs. (17) and (18) and consequently the perturbations increase (decrease) with time. For each set of parameters analyzed there is only one root for ω that makes negative the real parts of both eigenvalues of $\mathcal{A}$. Thus it defines the actual stable propagating solution. This root is explicitly given in Eq. (A9) in the Appendix.

Figure 7 makes a comparison of the analytical weakly nonlinear prediction for the final propagating velocity from Eq. (A9) (plotted as continuous curves) with the one obtained by numerically solving the differential equations (17) and (18) (plotted as dots). Also shown is the linear prediction for the fastest growing mode phase velocity $\mathrm{Im}[-\Lambda(k_{\max})/k_{\max}]$ displayed as dotted curves. This is done to investigate the plausibility of the purely linear approximation. Here we plot v_f as a function of α for three values of $N_B = 20,25,30$ with black, dark gray, and light gray curves, respectively. Since we are considering the case where $c_0 = 0$, there are only contributions to v_f that come from the tilted magnetic field. The vertical dashed lines indicate the critical values of α below which the interface is stable and remains flat. As we can see, the curves reach a maximum of v_f for a value of α greater than the critical one and then tend to zero as α approaches

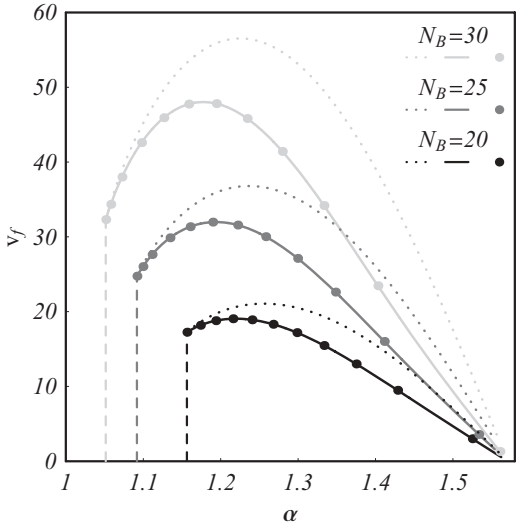

FIG. 7. Propagating final velocity v_f as a function of α for $c_0 = 0$, $N_B = 20$ (black), $N_B = 25$ (dark gray), and $N_B = 30$ (light gray). The dotted curves depict the linear prediction of the fastest growing mode phase velocity, the solid curves correspond to the analytical weakly nonlinear prediction, and the dots show the velocities obtained by numerically evaluating the time evolution of Eqs. (17) and (18). The dashed vertical lines indicate the critical values of α.

$\pi/2$, when there is no magnetic field tilting. In addition, it is observed that for any value of α the final velocity gets larger when N_B is increased. Thus, by tuning α and N_B one can control v_f.

By comparing the solid curves with the dotted ones we notice that the linear prediction works well when α is near its critical value or near $\pi/2$. This can be understood by the observation that near the critical value of α only the fundamental mode $k_{\max}$ has a noticeable amplitude and there is effectively just one mode acting and thus negligible nonlinear coupling. For higher values of α there is a relevant difference between the weakly nonlinear and the linear predictions, indicating that the coupling between the $k_{\max}$ and its harmonic is significant. Moreover, for α near $\pi/2$ there is no second-order contribution to the propagation, so the agreement with the linear prediction is good again. In contrast, by comparing the solid curves with the dots, we verify that there is excellent agreement between the analytical weakly nonlinear predictions and the numerical results. Therefore, we conclude that the coupling between the modes plays a fundamental role in determining the final propagation velocity.

IV. CONCLUSION

Parallel flow in a Hele-Shaw cell occurs when two immiscible viscous fluids flow with relative velocity parallel to the interface between them. By considering one of the fluids as a ferrofluid, we examined the influence of an in-plane tilted magnetic field on the profile shape and propagation velocity of interfacial traveling waves. We performed a weakly nonlinear analysis of the system that provides important analytic insight into the dynamics of the propagating structures. This is accomplished by utilizing a small number of coupled Fourier modes at the lowest nonlinear order.

The action of the tilted magnetic field is revealed already at the linear regime: It is shown that by tilting the field one can sustain wave motion even in the absence of external flow. Moreover, it is found that the velocity of the waves depends on the tilting angle. Our nonlinear results indicate that the time evolving interfacial wave shapes tend to approach stationary wave profiles. In fact, the shape of such stationary wavy patterns can be manipulated by the tilted magnetic field, resulting in different nonlinear wave forms: sinusoidal, vertical peaked structures separated by wide troughs, and skewed undulating forms. Finally, we found that the nonlinear wave velocity is sensitive to variations on the tilting angle, a mechanism that can be used to control its magnitude.

It would be of interest to see our theoretical results verified by laboratory experiments. However, we are not aware of any existing parallel flow experiment with a ferrofluid subject to a tilted uniform magnetic field. Interestingly, there is a recent example in the literature in which a theoretical prediction [26] about solitary wave propagation in ferrofluids has been realized experimentally [27]. However, it considered the action of an azimuthal magnetic field on a cylindrical ferrofluid surface. In the same spirit, we hope our current results could pave the way for future experimental and theoretical investigations into propagating deformations and localized waves in Hele-Shaw parallel flow with ferrofluids.

ACKNOWLEDGMENTS

We thank Brazilian Research Council (CNPq) for financial support through the Instituto Nacional de Ciência e Tecnologia de Fluidos Complexos program and also through the CNPq/FAPESQ Pronex program.

APPENDIX: NONLINEAR VELOCITY CALCULATION

In this Appendix we present the details of the analytical calculation for the nonlinear wave velocity v_f. We begin by substituting the ansatz expressions $\zeta_k(t) = c_1 \exp(-i\omega t)$ and $\zeta_{2k}(t) = c_2 \exp(-i2\omega t)$ in Eqs. (17) and (18) to obtain the following equations involving c_1, c_2, and ω:

$$\omega = i\Lambda(k) + ic_2\{F(k,-k) + F(k,2k) + i[G(k,-k) - G(k,2k)]\omega\}, \tag{A1}$$

$$2\omega c_2 = i\Lambda(2k)c_2 + ic_1^2[F(2k,k) - iG(2k,k)\omega], \tag{A2}$$

where we have used that $\zeta_{-k}(t) = \zeta_k^*(t)$ and $c_1 = c_1^*$, with the asterisk representing complex conjugation. By taking the real and imaginary parts of these equations and eliminating the variables c_1 and c_2, we find a third-order polynomial equation for ω,

$$a\omega^3 + b\omega^2 + c\omega + d = 0, \tag{A3}$$

whose coefficients are real and are given by

$$a = \mathrm{Re}([G(k,-k) - G(k,2k)]\{2F(2k,k) + G(2k,k)[2\Lambda(k) + \Lambda(2k)]\} - 2G(2k,k)[F(k,-k) + F(k,2k)]), \tag{A4}$$

$$b = \mathrm{Im}([F(k,-k) + F(k,2k)]\{2F(2k,k) + G(2k,k)[2\Lambda^*(k) + \Lambda^*(2k)]\} + [G(k,-k) - G(k,2k)]\{F^*(2k,k)[2\Lambda(k) + \Lambda(2k)] + G(2k,k)\Lambda(k)\Lambda(2k)\}), \tag{A5}$$

$$c = \mathrm{Re}([F^*(k,-k) + F^*(k,2k)]\{G(2k,k)\Lambda(k)\Lambda(2k) + F^*(2k,k)[2\Lambda(k) + \Lambda(2k)]\} - [G(k,-k) - G(k,2k)]F^*(2k,k)\Lambda(k)\Lambda(2k)), \tag{A6}$$

$$d = \mathrm{Im}\{[F^*(k,-k) + F^*(k,2k)]F^*(2k,k)\Lambda(k)\Lambda(2k)\}. \tag{A7}$$

The problem is further simplified by noticing that Eq. (14) imposes that $G(k,2k) = G(2k,k) = 0$. The discriminant of Eq. (A3) is

$$\Delta = 18abcd - 4b^3d + b^2c^2 - 4ac^3 - 27a^2d^2, \tag{A8}$$

which is always positive for the range of physical parameters considered in this work [5,19]. As a result, there are three distinct real roots given by

$$\omega_1 = -\frac{b}{3a} + \frac{(1 - i\sqrt{3})(-b^2 + 3ac)}{32^{2/3}ap} - \frac{(1 + i\sqrt{3})p}{32^{4/3}a}, \tag{A9}$$

$$\omega_2 = -\frac{b}{3a} + \frac{(1 + i\sqrt{3})(-b^2 + 3ac)}{32^{2/3}ap} - \frac{(1 - i\sqrt{3})p}{32^{4/3}a}, \tag{A10}$$

$$\omega_3 = -\frac{b}{3a} + \frac{2^{1/3}(-b^2 + 3ac)}{3ap} - \frac{p}{32^{1/3}a}, \tag{A11}$$

where

$$p = \Big[-2b^3 + 9abc - 27a^2d + \sqrt{4(-b^2+3ac)^3 + (-2b^3+9abc-27a^2d)^2}\Big]^{1/3}. \quad \text{(A12)}$$

By performing a stability analysis for each of these roots, as described in Sec. III C, we verify that ω_1 is the only one that is indeed stable. Therefore, the solution related to ω_1 [Eq. (A9)] is the one that prevails from the system dynamics, so the observed final nonlinear propagating velocity is given by $v_f = \omega_1/k$.

[1] P. G. Saffman and G. I. Taylor, Proc. R. Soc. London Ser. A **245**, 312 (1958).
[2] G. Homsy, Annu. Rev. Fluid Mech. **19**, 271 (1987); K. V. McCloud and J. V. Maher, Phys. Rep. **260**, 139 (1995); J. Casademunt, Chaos **14**, 809 (2004).
[3] M. Zeybek and Y. C. Yortsos, Phys. Rev. Lett. **67**, 1430 (1991).
[4] M. Zeybek and Y. C. Yortsos, J. Fluid Mech. **241**, 421 (1992).
[5] P. Gondret and M. Rabaud, Phys. Fluids **9**, 3267 (1997).
[6] L. Meignin, P. Gondret, C. Ruyer-Quil, and M. Rabaud, Phys. Rev. Lett. **90**, 234502 (2003).
[7] C. Ruyer-Quil, C. R. Acad. Sci., Ser. II B—Mec. **329**, 337 (2001).
[8] F. Plouraboué and E. J. Hinch, Phys. Fluids **14**, 922 (2002).
[9] E. J. Hinch and F. Plouraboué, Phys. Fluids **17**, 052107 (2005).
[10] J. A. Miranda and M. Widom, Phys. Rev. E **61**, 2114 (2000).
[11] R. E. Rosensweig, *Ferrohydrodynamics* (Cambridge University Press, Cambridge, 1985).
[12] E. Blums, A. Cebers, and M. M. Maiorov, *Magnetic Fluids* (de Gruyter, New York, 1997).
[13] For recent reviews on ferrofluids see, for instance, D. Andelman and R. E. Rosensweig, J. Phys. Chem. B **113**, 3785 (2009); J.-C. Bacri and F. Elias, in *Morphogenesis—Origins of Patterns and Shapes*, edited by P. Bourgine and A. Lesne (Springer, New York, 2011).
[14] J. A. Miranda and M. Widom, Int. J. Mod. Phys. B **12**, 931 (1998).
[15] J. A. Miranda and M. Widom, Physica D **120**, 315 (1998).
[16] A. O. Tsebers, Magnetohydrodynamics (NY) **17**, 113 (1981).
[17] D. P. Jackson, R. E. Goldstein, and A. O. Cebers, Phys. Rev. E **50**, 298 (1994).
[18] S. A. Lira and J. A. Miranda, Phys. Rev. E **84**, 016303 (2011).
[19] C. Flament, S. Lacis, J.-C. Bacri, A. Cebers, S. Neveu, and R. Perzynski, Phys. Rev. E **53**, 4801 (1996).
[20] S. Orzag, J. Fluid Mech. **50**, 689 (1971).
[21] T. Tatsumi and T. Yoshimura, J. Fluid Mech. **212**, 437 (1990).
[22] A. O. Tsebers and M. M. Maiorov, Magnetohydrodynamics (NY) **16**, 21 (1980).
[23] S. A. Langer, R. E. Goldstein, and D. P. Jackson, Phys. Rev. A **46**, 4894 (1992).
[24] J. Richardi, D. Ingert, and M. P. Pileni, Phys. Rev. E **66**, 046306 (2002).
[25] J. Richard and M. P. Pileni, in *Advanced Topics in Theoretical Chemical Physics*, Progress in Theoretical Chemistry and Physics, edited by J. Maruani, R. Lefebvre, and E. Brandas, Vol. 12 (Kluwer Academic Publishers, Dordrecht, The Netherlands, 2003), pp. 41–50.
[26] D. Rannacher and A. Engel, New J. Phys. **8**, 108 (2006).
[27] E. Bourdin, J.-C. Bacri, and E. Falcon, Phys. Rev. Lett. **104**, 094502 (2010).